Computer Simulation of a Squirrel-Cage Induction Machine with Non-Linear Effects

Dr. -Ing. O. I. Okoro

Department of Electrical Engineering, University of Nigeria, Nsukka, Enugu State, Nigeria.
Email: ogbonnayaokoro@hotmail.com

ABSTRACT

The paper presents the dynamic modelling and computer simulation of a squirrel-cage induction machine with non-linear effects. The computer simulation for the transient operation is obtained from the non-linear differential system of equations, which describe the induction machine in the rotor reference frame and with currents as state variables. It is shown that by using the characteristic data available from D.C. measurement, No-load, Blocked Rotor and Retardation tests of the machine as well as the results obtained from the optimisation of the T-model rotor circuit, accurate simulation of the machine under dynamic conditions is possible. The simulated time function of the transient current, mechanical speed and shaft torque characteristics of the machine are compared with the experimental results.

(Key words: dynamic modelling, currents, numerical integration technique, current, no-load, blocked rotor, retardation test, shaft torque)

INTRODUCTION

The need for a simple, accurate and faster method of simulating the transient performances of induction machines has become imperative due to the wide industrial applications of these machines. In the past, analog computers have been used to study the system dynamics of induction machines [1,2]. This method is, however, well suited for D.C. machines since analog computers are well adapted to handling direct voltages. A problem therefore arises when analog computers are used in the simulation of the A.C. induction machine in dynamic systems. In [3], a software package was developed using the FORTRAN programming language and the predictor-corrector numerical technique, for the dynamic simulation of induction motor drives. Chattopadhyay [4] uses the numerical integration technique of Runge-Kutta-Merson to simulate an adjustable-speed induction motor drive. Both of these techniques require the development of numerical integration and inversion routines for the solution of the resultant non-linear differential equations that describe the dynamic behaviour of the machine. It will be shown in this paper that the development of such a user-written program for the purpose of simulating the dynamic behaviour of A.C. induction machine is not necessary and that a commercial software package such as MATLAB® [5], licensed by Mathworks, presents a better alternative. By incorporating FORTRAN or C compilers, the problem of execution speed is alleviated. In MATLAB®, the integration algorithms and inversion function are efficient and accurate thereby saving the time and energy that could have been used in programming. This paper therefore uses MATALB® to develop computer program that can simulate and solve the non-linear differential equations which describe the dynamic behaviour of a squirrel-cage induction machine with saturation and skin effects. Simulation results which show the free-acceleration of the machine in rotor reference frame as well as the experimental results are presented and discussed.

INDUCTION MACHINE MODEL WITH SKIN-EFFECT

In order to accurately represent the skin-effect phenomenon in a squirrel-cage induction machine, two distinct methods have been proposed. The quasi-static method in which the steady state values of resistance and inductance are first calculated for each speed within the operating range represents the first [6,7]. The second method represents the eddy-currents by additional circuit equations. The equations may be in the form of lumped-parameter networks, which are effectively a crude finite difference approximation to the field equations describing the eddy-current distribution [8].

The first method produces unacceptable results at high frequencies. In this paper, therefore, the lumped-parameter networks model is applied. In order to account for changes of the rotor inductance and resistance with changes in frequency, the rotor bar is divided into sections as shown in Figure 1.

To model the rotor bar, a T-configuration network is used according to the method

proposed by Babb and Williams [8]. From Figure 1, the rotor bar resistance and inductance for each section is:

$$R_{\sec} = \frac{L_s}{\chi_{cu} h_{\sec} b_{Nut}} \quad (1)$$

$$L_{\sec} = \frac{\mu_o L_s h_{\sec}}{b_{Nut}} \quad (2)$$

where, μ_o = Permeability of free space and b_{Nut} = Width of the rotor bar.

It is important to note that equations (1) and (2) are modified to take account of all the bars and subsequently referred to the stator to give "Rr" and "Lr" as shown in the equivalent T-circuit of the induction motor, Figure 1b and Figure 1c.

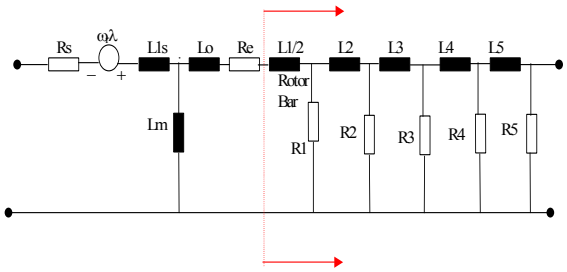

Figure 1a: Equivalent T-Circuit; Configuration for 5-section rotor bar.

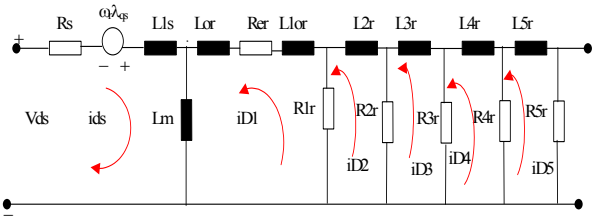

Figure 1b: Equivalent circuit for d-axis with rotor values referred to the stator

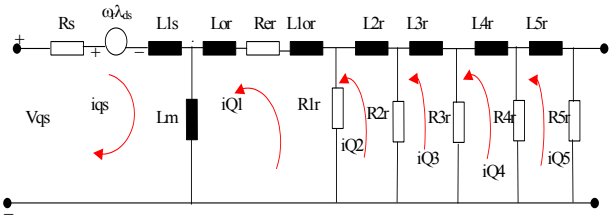

Figure 1c: Equivalent circuit for q-axis with rotor values referred to the stator

The machine d-q model equations are derived by taken from the Kirchhoff's voltage expressions for each loop in Figure 6.1 [9]. By using the reference frame fixed to the rotor, the voltage equations for each of the loops become:

[A] Stator Equations—(Fig. 1b & Fig. 1c)

Loop1

$$Vds = Rsi_{ds} + Ls\frac{di_{ds}}{dt} - Ls\omega_r i_{qs} - Lm\omega_r iQ1 + Lm\frac{diD1}{dt} \quad (3)$$

$$Vqs = Rsi_{qs} + \omega_r \lambda_{ds} + Lls\frac{di_{qs}}{dt} + Lm\frac{di_{qs}}{dt} + Lm\frac{diQ1}{dt} \quad (4)$$

[B] Rotor Equations-(Fig. 1b & Fig. 1c)

Loop2

$$VD1 = 0 = (\mathrm{Re}r + Rlr)iD1 - RlriD2 + Llr\frac{diD1}{dt} + Lm\frac{di_{ds}}{dt} + Lm\frac{diD1}{dt} \quad (5)$$

$$VQ1 = 0 = (\mathrm{Re}r + Rlr)iQ1 - Rlriq2 + Llr\frac{diQ1}{dt} + Lm\frac{di_{qs}}{dt} + Lm\frac{diQ1}{dt} \quad (6)$$

Loop3

$$VD2 = 0 = R1riD2 - R1riD1 + R2riD2 - R2riD3 + L2r\frac{diD2}{dt} \quad (7)$$

$$VQ2 = 0 = R1riQ2 - R1riQ1 + R2riQ2 - R2riQ3 + L2r\frac{diQ2}{dt} \quad (8)$$

Loop4

$$VD3 = 0 = R2riD3 + R3riD3 - R3riD4 - R2riD2 + L3r\frac{diD3}{dt} \quad (9)$$

$$VQ3 = 0 = R2riQ3 + R3riQ3 - R3riQ4 - R2riQ2 + L3r\frac{diQ3}{dt} \quad (10)$$

Loop5

$$VD4 = 0 = R4riD4 + R3riD4 - R3riD3 - R4riD5 + L4r\frac{diD4}{dt} \quad (11)$$

$$VQ4 = 0 = R4riQ4 + R3riQ4 - R3riQ3 - R4riQ5 + L4r\frac{diQ4}{dt} \quad (12)$$

Loop6

$$VD5 = 0 = R5riD5 + R4riD5 - R4riD4 + L5r\frac{diD5}{dt} \quad (13)$$

$$VQ5 = 0 = R5riQ5 + R4riQ5 - R4riQ4 + L5r\frac{diQ5}{dt} \quad (14)$$

MODEL DEVELOPMENT WITH SATURATION EFFECT

The values of the inductances used in the development of the dynamic equations for the classical and skin-effect induction machine models were assumed to be constant. By so doing, the models fail to take into consideration the saturation effects of the magnetizing field. It has been proved beyond doubts by several authors [10,11,12,13] that the stability and dynamic conditions of an induction machine are highly affected by saturation. Several methods have been developed in modelling saturation effects in induction machines [13,14,15,16,17], each differing in the area of application, and of course, in the part of the machine inductances

that are assumed to saturate. In [13,14], induction motors with saturable leakage reactances are modelled and simulated with the help of analog computer and IGSPICE respectively. In He [12] and Levi [16] the effect of considering the main flux saturation is investigated. A saturation model for leakage inductances presents a difficult task in terms of analysis and computer time [13,14,17]. It has been shown, however, that the main magnetizing field contributes significantly to the disparity between induction machine computer simulation results and experimental results [12]. Therefore, to a very high level of accuracy, the effects of saturation in induction machines can be included by variation of the main flux inductance while assuming the leakage inductances to be constant. However, where the stator and rotor currents are expected to be very high values, inclusion of the leakage inductance saturation becomes imperative [13,14]. In this paper, saturation due to the influence of the main flux inductance is considered. The application of this method requires that the no-load saturation curve of the machine be known. The saturation curve of the induction motor determined by taking the motor no-load current measurements with balanced 3-phase, 50 Hz voltages applied to the stator windings without mechanical load on the motor is shown in Figure 2.

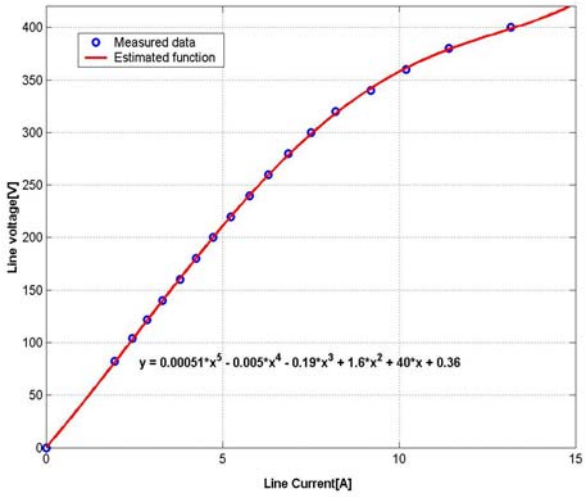

Figure 2: No-Load Saturation curve.

The voltage increments start below rated voltage on the linear portion of the curve and normally continue to somewhat above rated voltage well beyond the knee of the curve. It is important to add that measurements above rated voltage should be taken as quickly as possible to avoid over heating of the stator windings and consequent causing the breakdown of the machine. Because the loss component of the no-load current is very low compared to the magnetizing component, the measured no-load current values may be assumed to be all flux-producing currents without loss in accuracy. Due to the very low slip at no-load, the secondary branch impedances become very high relative to the stator. This practically eliminates the participation of the rotor circuit, leaving only the stator leakage (Lls) and the magnetizing branch (Lm) to contribute to the no-load saturation curve shown in Figure 2. Since the stator leakage inductance, Lls is assumed as constant, the magnetizing inductance can be extracted from Figure 2. By so doing, Figure 3 results:

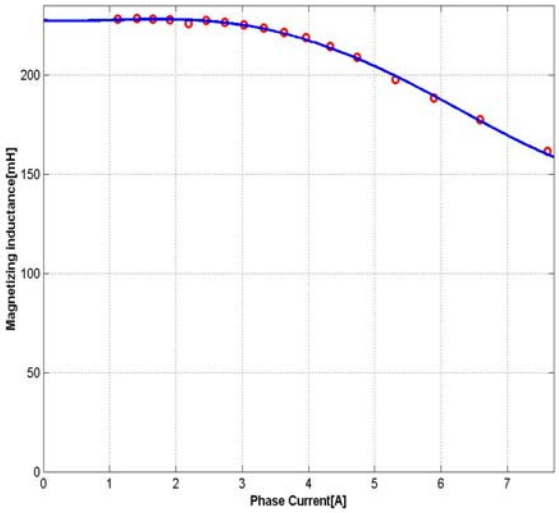

Figure 3: Saturation characteristic curve.

In order to find an analytical expression for the saturation characteristic curve of Figure 3, a curve-fitting method which employs the algorithm of Marquardt [18] is employed. Figure 4 shows the approximated curve with the estimated function as:

$$Lm = 0.064 i_m^4 - 0.94 i_m^3 + 2.4 i_m^2 - 1.4 i_m + 230 \; [mH] \quad \textbf{(15)}$$

By storing the analytical expression in the computer, the value of the magnetizing inductance in the Skin-effect model can be updated at each integration step.

MODEL EQUATIONS IN STATE VARIABLE FORM

In order to facilitate the digital computer simulation of the developed model, it is necessary to put the differential equations representing both the electrical and mechanical models of the machine in its state variable form. The electrical model of the machine with currents as state variables becomes:

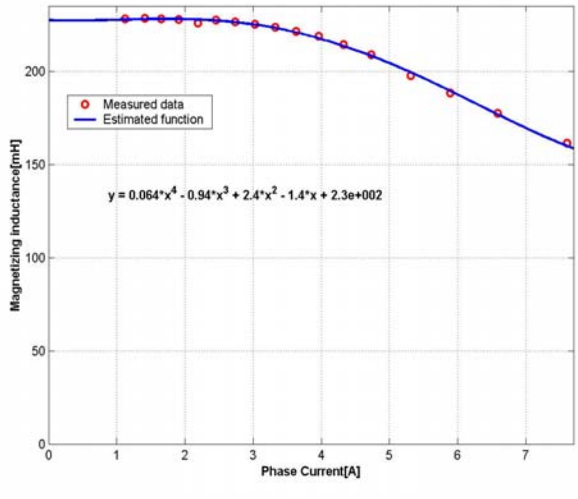

Figure 4: Saturation Curve and Polynomial approximation.

$$[\mathbf{V}] = [\mathbf{R}][\mathbf{i}] + [\mathbf{L}]\frac{d[\mathbf{i}]}{dt} + \omega_r[\mathbf{G}][\mathbf{i}] \qquad \textbf{(19)}$$

But $\dot{\mathbf{X}} = \mathbf{AX} + \mathbf{BU}$ **(20)**

Therefore, equation (19) can be rearranged to arrive at the following:

$$\frac{d[\mathbf{i}]}{dt} = -[\mathbf{L}]^{-1}([\mathbf{R}] + \omega_r[\mathbf{G}])[\mathbf{i}] + [\mathbf{L}]^{-1}[\mathbf{V}] \qquad \textbf{(21)}$$

Comparing equation (20) and equation (21), we have:

$$\mathbf{A} = -[\mathbf{L}]^{-1}([\mathbf{R}] + \omega_r[\mathbf{G}]) \qquad \textbf{(22a)}$$

$$\mathbf{B} = [\mathbf{L}]^{-1} \qquad \textbf{(22b)}$$

$$\mathbf{U} = [\mathbf{V}] \qquad \textbf{(22c)}$$

$$\mathbf{X} = [\mathbf{i}] \qquad \textbf{(22d)}$$

Where **R, L,V,i** and **G** are defined as:

$$[\mathbf{i}] = [i_{ds} \; i_{qs} \; iD1 \; iQ1 \; iD2 \; iQ2 \; iD3 \; iQ3 \; iD4 \; iQ4 \; iD5 \; iQ5]^t \qquad \textbf{(23)}$$

$$[\mathbf{V}] = [Vds \; Vqs \; 0 \; 0 \; 0 \; 0 \; 0 \; 0 \; 0 \; 0 \; 0 \; 0]^t \qquad \textbf{(24)}$$

$$[\mathbf{G}] = \begin{bmatrix} 0 & -Ls & 0 & -Lm & 0 & 0 & 0 & 0 & 0 & 0 & 0 & 0 \\ Ls & 0 & Lm & 0 & 0 & 0 & 0 & 0 & 0 & 0 & 0 & 0 \\ 0 & 0 & 0 & 0 & 0 & 0 & 0 & 0 & 0 & 0 & 0 & 0 \\ 0 & 0 & 0 & 0 & 0 & 0 & 0 & 0 & 0 & 0 & 0 & 0 \\ 0 & 0 & 0 & 0 & 0 & 0 & 0 & 0 & 0 & 0 & 0 & 0 \\ 0 & 0 & 0 & 0 & 0 & 0 & 0 & 0 & 0 & 0 & 0 & 0 \\ 0 & 0 & 0 & 0 & 0 & 0 & 0 & 0 & 0 & 0 & 0 & 0 \\ 0 & 0 & 0 & 0 & 0 & 0 & 0 & 0 & 0 & 0 & 0 & 0 \\ 0 & 0 & 0 & 0 & 0 & 0 & 0 & 0 & 0 & 0 & 0 & 0 \\ 0 & 0 & 0 & 0 & 0 & 0 & 0 & 0 & 0 & 0 & 0 & 0 \\ 0 & 0 & 0 & 0 & 0 & 0 & 0 & 0 & 0 & 0 & 0 & 0 \\ 0 & 0 & 0 & 0 & 0 & 0 & 0 & 0 & 0 & 0 & 0 & 0 \end{bmatrix} \qquad \textbf{(25)}$$

$$[\mathbf{R}] = \begin{bmatrix} Rs & 0 & 0 & 0 & 0 & 0 & 0 & 0 & 0 & 0 & 0 & 0 \\ 0 & Rs & 0 & 0 & 0 & 0 & 0 & 0 & 0 & 0 & 0 & 0 \\ 0 & 0 & R11 & 0 & -R1r & 0 & 0 & 0 & 0 & 0 & 0 & 0 \\ 0 & 0 & 0 & R11 & 0 & -R1r & 0 & 0 & 0 & 0 & 0 & 0 \\ 0 & 0 & -R1r & 0 & R22 & 0 & -R2r & 0 & 0 & 0 & 0 & 0 \\ 0 & 0 & 0 & -R1r & 0 & R22 & 0 & -R2r & 0 & 0 & 0 & 0 \\ 0 & 0 & 0 & 0 & -R2r & 0 & R33 & 0 & -R3r & 0 & 0 & 0 \\ 0 & 0 & 0 & 0 & 0 & -R2r & 0 & R33 & 0 & -R3r & 0 & 0 \\ 0 & 0 & 0 & 0 & 0 & 0 & -R3r & 0 & R44 & 0 & -R4r & 0 \\ 0 & 0 & 0 & 0 & 0 & 0 & 0 & -R3r & 0 & R44 & 0 & -R4r \\ 0 & 0 & 0 & 0 & 0 & 0 & 0 & 0 & -R4r & 0 & R55 & 0 \\ 0 & 0 & 0 & 0 & 0 & 0 & 0 & 0 & 0 & -R4r & 0 & R55 \end{bmatrix} \qquad \textbf{(26)}$$

Where,

$$R11 = \mathrm{Re}\,r + R1r \qquad \textbf{(27a)}$$

$$R22 = R1r + R2r \qquad \textbf{(27b)}$$

$$R33 = R2r + R3r \qquad \textbf{(27c)}$$

$$R44 = R3r + R4r \qquad \textbf{(27d)}$$

$$R55 = R4r + R5r \qquad \textbf{(27e)}$$

$$[\mathbf{L}] = \begin{bmatrix} Ls & 0 & Lm & 0 & 0 & 0 & 0 & 0 & 0 & 0 & 0 & 0 \\ 0 & Ls & 0 & Lm & 0 & 0 & 0 & 0 & 0 & 0 & 0 & 0 \\ Lm & 0 & Lmr & 0 & 0 & 0 & 0 & 0 & 0 & 0 & 0 & 0 \\ 0 & Lm & 0 & Lmr & 0 & 0 & 0 & 0 & 0 & 0 & 0 & 0 \\ 0 & 0 & 0 & 0 & L2r & 0 & 0 & 0 & 0 & 0 & 0 & 0 \\ 0 & 0 & 0 & 0 & 0 & L2r & 0 & 0 & 0 & 0 & 0 & 0 \\ 0 & 0 & 0 & 0 & 0 & 0 & L3r & 0 & 0 & 0 & 0 & 0 \\ 0 & 0 & 0 & 0 & 0 & 0 & 0 & L3r & 0 & 0 & 0 & 0 \\ 0 & 0 & 0 & 0 & 0 & 0 & 0 & 0 & L4r & 0 & 0 & 0 \\ 0 & 0 & 0 & 0 & 0 & 0 & 0 & 0 & 0 & L4r & 0 & 0 \\ 0 & 0 & 0 & 0 & 0 & 0 & 0 & 0 & 0 & 0 & L5r & 0 \\ 0 & 0 & 0 & 0 & 0 & 0 & 0 & 0 & 0 & 0 & 0 & L5r \end{bmatrix} \qquad \textbf{(28)}$$

Where,

$$Lmr = L1r + Lm \qquad \textbf{(29)}$$

The Electromagnetic torque,Te is given as:

$$T_e = \frac{3}{2}PL_m\left(i_{qs}i_{dr} - i_{ds}i_{qr}\right) \qquad \textbf{(30)}$$

where, P=Number of pole pairs.

The mechanical model of the machine including the coupling system but with damping factor (d_w) neglected can be expressed as in [19]:

$$\begin{bmatrix} \dot{\omega}_m \\ \dot{\omega}_{mL} \\ \dot{M}_w \end{bmatrix} = \begin{bmatrix} 0 & 0 & -\frac{1}{J_{m1}} \\ 0 & 0 & \frac{1}{J_L} \\ c_w & -c_w & 0 \end{bmatrix} \begin{bmatrix} \omega_m \\ \omega_{mL} \\ M_w \end{bmatrix} + \begin{bmatrix} \frac{T_e}{J_{m1}} \\ -\frac{T_L}{J_L} \\ 0 \end{bmatrix} \quad (31)$$

where J_{m1} , M_w J_L , c_w and ω_{mL} are moment of inertia of the induction motor, shaft torque, moment of inertia of the D.C. motor, = stiffness constant of the shaft system, mechanical speed of the D.C. motor respectively. The block diagram of equation (31) is shown in Figure 5.

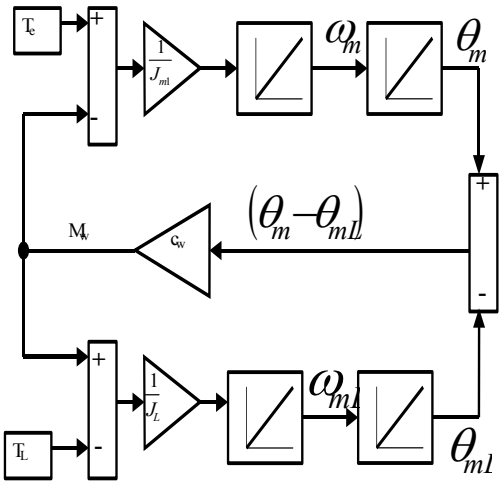

Figure 5. Block diagram of motor mechanical model with coupling.

EXPERIMENTAL VERIFICATION

The test machine is a **KATT VDE 0530**, Class F insulation, surfaced-cooled, squirrel-cage induction motor. The rated power, speed, and current are 7.5 KW, 1400 rpm and 19.2 A, respectively. The test machine is a four-pole motor with 50 Hz rated frequency and 340 V rated voltage. Figure 6 shows the test machine.

Several experiments were carried out on the test machine. The No-load test was carried out at rated frequency and with balanced poly-phase voltages applied to the stator terminals. Readings for current, voltage, electrical power and speed were taken after the motor has been running for a considerable long period of time necessary for the bearings to be properly lubricated. Locked-rotor test and test with the injection of D.C. current in the stator windings were made at standstill. The test with the injection of D.C. current in the stator windings

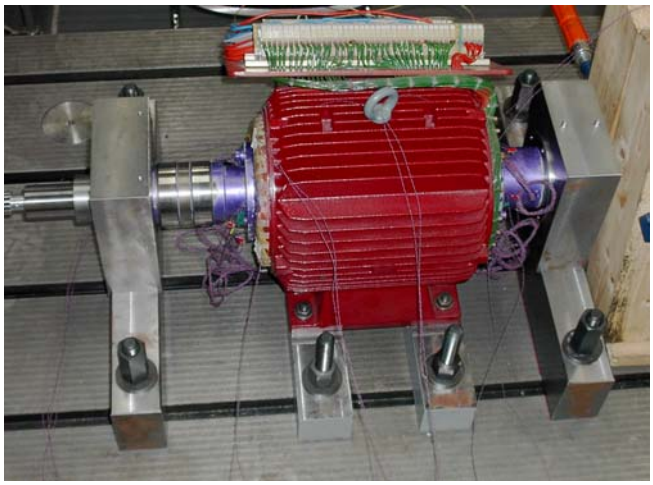

Figure 6: The 7.5KW test motor.

were made at standstill. The retardation test was carried out at No-load with and without additional standard mass. The load test was carried out with constant load and frequency at a sinusoidal stator windings voltage. The test machine is star-delta connected, operated as motor and was loaded by 7.6KW D.C. machine as shown in Figure 7.

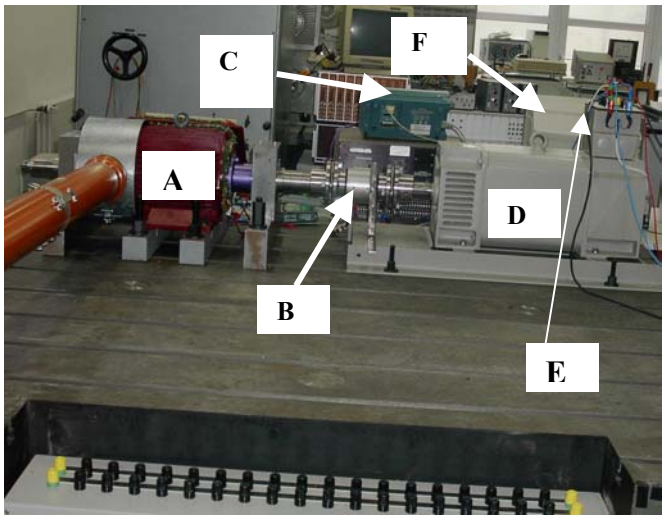

Figure 7: Test machine experimental set-up during rated load operation.

Figure 7 labels: Test machine (A), Coupling system (B), Digital-Real-Time Oscilloscope (C), Load D.C. machine(D), Mechanical speed leads(E), Computer(F)

Measurements of the test machine's transient stator currents, stator voltages, shaft torque and speed were made during run-up of the machine. The mechanical speed leads (E) as shown in Figure 7 were taken through the speed terminals of the tacho-generator and connected to one of the channels of Digital Real-Time Oscilloscope,

DRTO (C). The tacho-generator analog output is 20 V per 1000 rpm. The shaft torque was measured by using the 22/100 DATAFLEX torque measuring instrument connected together with the coupling system (B). The torque measuring instrument has as its output voltage which was read through the DRTO. Three FLUKE current probes but with the same setting were used to measure the transient stator phase currents at run-up operation. All the run-up operation measurements were recorded in real time via a four-channel TS 200-series DRTO with RS232 output terminal. The RS232 output terminal enables the output from the DRTO to be monitored through a computer (F).

INDUCTION MACHINE MODEL SIMULATION

In order to simulate the induction motor transient model, the differential equation (21), together with equation (15), equation (30) and equation(31)—which gives the mechanical behaviour of the motor are solved by developing MATLAB®[5] m-files which incorporate an in-built numerical algorithm, ODE45-a program that uses Runge-Kutta numerical method. The simulations have been carried out using the motor data obtained from the open circuit, short circuit, D.C. measurement and retardation tests of the motor under study (Appendix A) and the estimated rotor parameters (Appendix B). An optimisation algorithm is incorporated into the m-files from which the estimated rotor parameters are obtained. The optimised model as shown in Figure 8 closely matches with the actual rotor bar characteristics of the machine. At approximately 4 KHz frequency, the error in the developed model is about 6%.

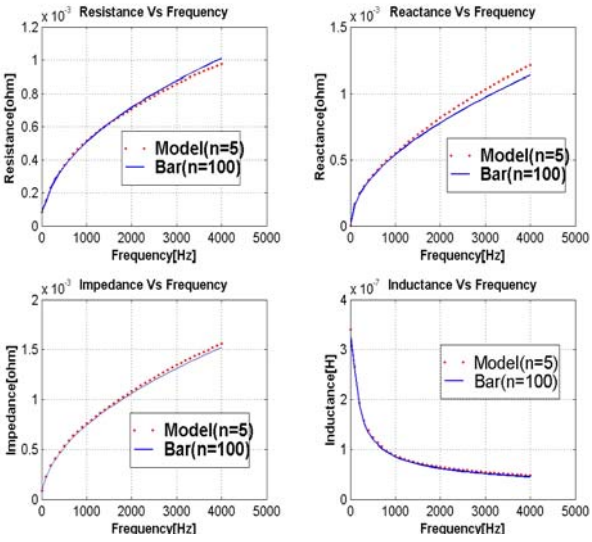

Figure 8: Bar-Model plots for bar sections (100) and model sections(5).

Figure 9 shows the predicted transient characteristics of the test machine during free acceleration with skin and saturation effects.

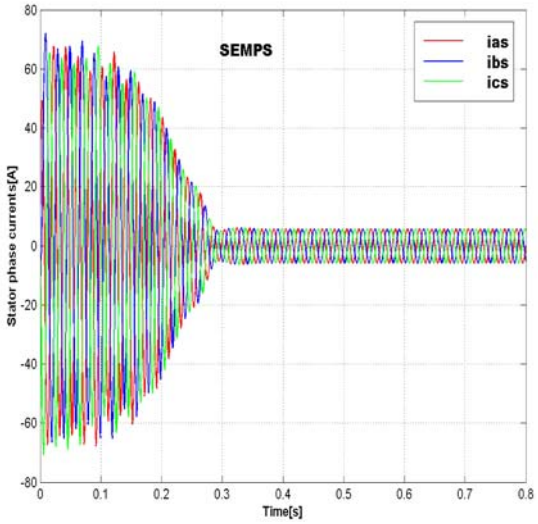

Figure 9a: Skin-effect model plus saturation (SEMPS) simulation: Stator phase currents at run-up.

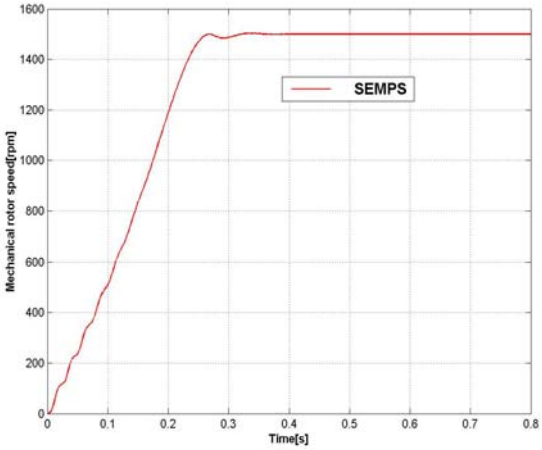

Figure 9b: Skin-effect model plus saturation (SEMPS) simulation: Mech. rotor speed at run-up.

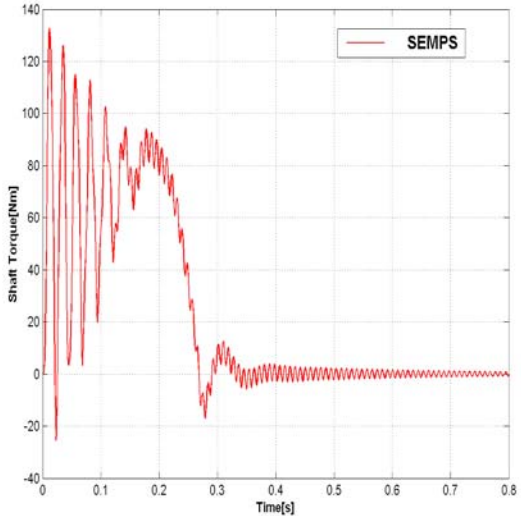

Figure 9c: Skin-effect model plus saturation (**SEMPS**) simulation: Shaft torque at run-up.

Figure 10 shows the measured run-up transient characteristics of the test machine. Comparison between Figures 9 and 10 shows that the predicted results closely match the measured results. However, the errors that exist in the predicted results may be as a result of the stator and rotor resistances which were assumed to be constant throughout the transient operation. This may not be necessarily so as the resistances are dependent on temperature—which in itself increases as the machine is in operation. Again, it is envisaged that consideration of the leakage inductances as being saturated may improve the simulated results. The mechanical model of the machine has been developed neglecting the damping factor and the friction in the bearing system. This definitely will diminish the accuracy of the predicted shaft torque.

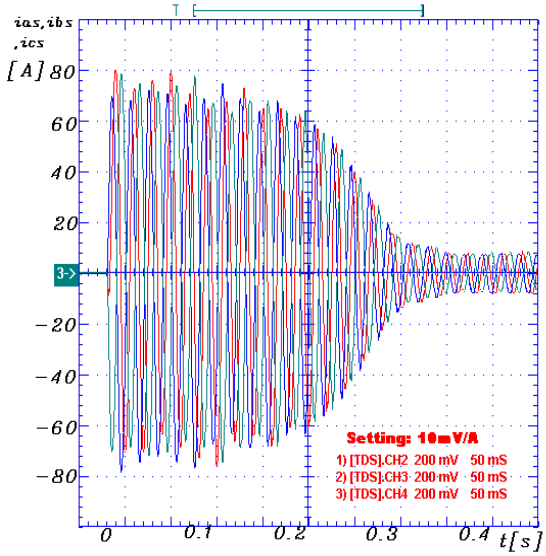

Figure 10a: Measurement: Stator phase currents at run-up (Delta connected, Vrms = 340 V).

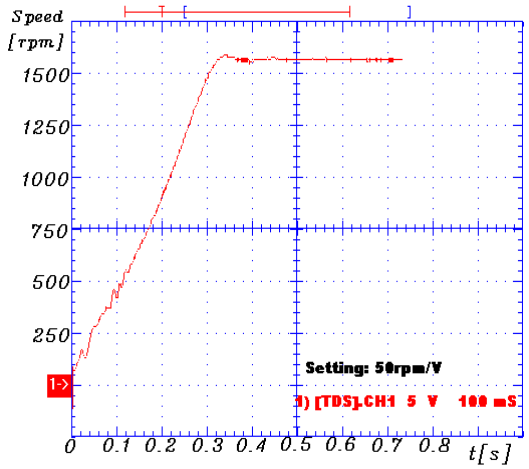

Figure 10b: Measurement: Mechanical rotor speed at run-up (Delta connected, Vrms=340V).

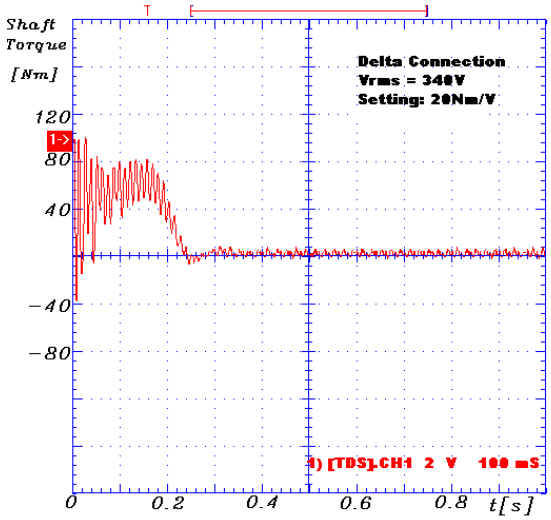

Figure 10c: Measurement: Shaft torque at run-up (Delta connected, Vrms = 340 V, Setting:20 Nm/V).

CONCLUSION

The paper has shown that the MATLAB® software package is highly suitable for the dynamic simulation of induction machine model with saturation and skin effects. By optimizing the rectangular-shaped rotor bar, a good correction between the model impedance and the actual rotor bar impedance could be achieved. The simulated machine model with saturation and skin effects included gives comparatively good result and can therefore be conveniently used to predict the actual machine performances in dynamic states. However, by making the stator and rotor resistances temperature dependent and by incorporating the damping factor and frictional loss coefficients in the mechanical systems equations, better results could be achieved.

REFERENCES

[1.] Jordan, H.E.: Analysis of induction machines in dynamic systems. *IEEE Transactions on Power Apparatus and Systems*, Vol. PAS-84, No. 11, PP. 1050-1088, Nov; 1965.

[2.] Krause, P.C. and Thomas, C.H.: Simulation of symmetrical induction machinery. *IEEE Transactions on Power Apparatus and Systems*, Vol. PAS-84, No. 11, PP.1038-1053, Nov: 1965.

[3.] Jordan, H.E.: Digital computer Analysis of induction machines in dynamic systems. *IEEE Transactions on Power Apparatus and Systems*, Vol. PAS-86, No. 6, PP. 722-728, June; 1967.

[4.] Chahopadhyay, A.K.: Digital computer simulation of an adjustable-speed induction motor drive with a cycloconverter type thyristor-commutator in the rotor. *IEEE Transactions on Industrial Electronics and Control Instrumentation*, PP. 86-92, Feb; 1976.

[5.]"MATLAB User's Guide", The Mathworks, Inc,: Natick, NJ. 1991.

[6.] Haun, Andreas: Vergleich von Steuerverfahren für Spannungseinprägende Umrichter Zur Speisung von Käfigläufermotoren. Darmstädter Dissertation, Juli 1991.

[7.] Humpage, W.D. et. al: Dynamic response analysis of interconnected synchronous-asychnronous machine groups. *Proc. IEE,* 166, (2), PP. 2015-2027, 1969.

[8.] Babb, D.S. and Williams, J.E.: Network analysis of A.C. machine conductors. *AIEE Transactions,* Vol. 70, PP.2001-2005, 1951.

[9.] Guiliemin, E.A.: *Introductory Circuit Theory*. Wiley, New York, 1953.

[10.] Melkebeek, J.A.A.: Magnetizing-field saturation and dynamic behaviour of induction machines. Part 1: Improved calculation method for induction-machine dynamics. *IEE Proc.* Vol. 130, Pt. B, No.1, PP.1-9, January 1983.

[11.] de Mello, F. P. and Walsh, G.W.: Reclosing transients in induction motors with terminal capacitors. *AIEE Transactions*, PP. 1206-1213, Feb. 1961.

[12.] He,Yi-Kang and Lipo, T.A.: Computer Simulation of an induction machine with spatially dependent saturation. *IEEE Transactions on Power Apparatus and Systems*, Vol. PAS-103, No.4, PP.707-714, April 1984.

[13.] Lipo, T.A. and Consoli, A.: Modelling and simulation of induction motors with saturable leakage reactances. *IEEE Transactions on industry Applications*, Vol.IA-20, No.1, PP.180-189, Jan./Feb; 1984.

[14.] Keyhani, A. and Tsai, H.: IGSPICE simulation of induction machines with saturable inductances. *IEEE Transactions on Energy Conversion*, Vol. 4, No.1, PP. 118-125, March 1989.

[15.] Boldea, I. and Nasar, S. A.: A general Equivalent circuit(GEC) of electric machines including cross-coupling saturation and frequency effects. *IEEE Transactions on Energy Conversion*, Vol.3, PP.689-695, September 1988.

[16.] Levi, E.: A unified approach to main flux saturation modelling in D-Q axis models of induction machines. *IEEE Transactions on Energy Conversion*, Vol.10, No.3, PP. 455-460, September 1995.

[17.] Slemon, G.R.: Modelling of induction machines for electric drives. *IEEE Transactions on Industry Applications,* Vol.25, No.6, PP.1126-1131, Nov./Dec.1989.

[18.] Marquardt, D.W.: An Algorithm for least-square estimation of non-linear parameters. *J. Soc. Ind. Appl. Math*, Vol. 11, No.2, PP.431-441, June 1963.

[19.] Okoro, O.I.: *Dynamic and Thermal Modelling of Induction Machine with Non-linear Effects*. Kassel University Press, Kassel, Sept. 2002.

APPENDIX A. MACHINE DATA

Output Power	7.5KW
Rated voltage	340V
Winding connection	Delta
Number of Poles	4
Rated speed	1400rpm
Rated frequency	50Hz
Stator resistance	2.52195ohm
Stator leakage reactance	1.95145ohm
Rotor resistance	0.976292ohm
Rotor leakage reactance	2.99451ohm
Magnetizing reactance	55.3431ohm
Mechanical shaft torque	51.2636N.m
Estimated rotor inertia moment	0.117393Kgm^2
Rated current	19.2A
Moment of inertia of D.C. motor	0.10958Kgm^2
Shaft stiffness constant	14320Nm/rad

APPENDIX B. ESTIMATED ROTOR CIRCUIT PARAMETER

Resistance	**[mΩ]**	**Inductance**	**[μH]**
R_1	1.338	L_1	6.1150e-2
R_2	0.656	L_2	9.2940e-2
R_3	0.321	L_3	0.1896
R_4	0.179	L_4	0.3562
R_5	1.338	L_5	0.2596

ACKNOWLEDGEMENT

The author wishes to express his thanks to DAAD for financial support and to Prof. Dr.-Ing. B. Weidemann for his assistance in producing this paper.

ABOUT THE AUTHOR

Dr.–Ing. O.I. Okoro holds a Ph.D. in Electrical Machines from the University of Kassel, Germany where he conducted his research under a DAAD Scholarship. He currently lectures in the Department of Electrical Engineering at the University of Nigeria, Nsukka. His research interests are in the areas of dynamic simulation and control of induction machines as well as in the thermal and dynamic analysis of AC machines. He is a member of the IEEE.

SUGGESTED CITATION

Okoro, O.I. 2003. Computer Simulation of a Squirrel-Cage Induction Machine with Non-Linear Effects. *Greenwich Journal of Science and Technology*. 4(1):56-64.